Solid State Ionics 331 (2019) 89–95

Contents lists available at ScienceDirect

Solid State Ionics

journal homepage: www.elsevier.com/locate/ssi

$Li_{1.4}Al_{0.4}Ti_{1.6}(PO_4)_3$ nanoparticle-reinforced solid polymer electrolytes for all-solid-state lithium batteries

Lehao Liu, Lihua Chu, Bing Jiang, Meicheng Li*

State Key Laboratory of Alternate Electrical Power System with Renewable Energy Sources, School of Renewable Energy, North China Electric Power University, Beijing 102206, China

ARTICLE INFO

Keywords:
Composite polymer electrolyte
Ion conductivity
Mechanical property
Thermal stability
Solid-state battery

ABSTRACT

The applications of solid polymer electrolytes in all-solid-state Li-ion batteries are restricted by their low ion conductivities at room temperature and poor mechanical and thermal stabilities. Herein, $Li_{1.4}Al_{0.4}Ti_{1.6}(PO_4)_3$ (LATP) electrolyte nanoparticles were used as active fillers to improve the properties of polyethylene oxide (PEO)-based electrolytes. The ion conductivity of the composite electrolyte with 1 wt% LATP increased to 1.2×10^{-5} S/cm at room temperature, because of the effective inhibition of the PEO matrix crystallization by the high-conductivity LATP nanofillers. The electrochemical, mechanical and thermal stabilities were also enhanced by the LATP nanofillers. The LATP-filled composite electrolytes can effectively block Li dendrites in symmetric Li/electrolyte/Li cells during repeated Li stripping/plating with a current density of 0.10 mA/cm^2 for 600 h at 30 °C. Furthermore, the LATP-based all-solid-state $LiFePO_4$/Li cells exhibited higher reversible capacity (152 mAh/g at 0.10 C), cycling stability (84% after 20 cycles at 50 °C) and rate capability than the LATP-free cells.

1. Introduction

Li-ion batteries (LIBs) are widely used in portable devices, electric vehicles and gridding storage; however, the organic liquid electrolytes suffer from inadequate electrochemical and thermal stabilities and poor safety resulted from leakage, volatility, flammability, Li dendrite formation, dissolution of active materials and side reactions [1–7]. All-solid-state LIBs are regarded as one of the most promising next-generation rechargeable batteries, because the replacement of the liquid electrolytes by solid-state electrolytes cannot only eliminate the safety issues linked to the liquid electrolytes, but also offer the promising potentials of achieving higher energy density by using high-capacity electrodes such as high-voltage cathode, Li metal anodes and conversion-typed sulfur and oxygen electrodes [8–11]. The solid-state electrolytes also function as separators and thus may simplify battery fabrication processes [12].

Solid-state electrolytes are usually classified into inorganic ceramics and organic polymers. Considerable researches are focused on a few inorganic electrolytes with crystal structures such as $Li_{1+x}Al_xTi_{2-x}(PO_4)_3$ (LATP) and $Li_7La_3Zr_2O_{12}$ (LLZO), due to their combined merits of high conductivity (~10^{-4} S/cm at room temperature), wide electrochemical window and strong chemical stability in ambient atmosphere [13,14]. Nevertheless, their practical applications are mainly limited by the huge interfacial resistance between the rigid and brittle ceramic electrolytes and the electrodes caused by the poor contact and interface instability [15–17].

In contrast to the ceramic electrolytes, solid polymer electrolytes (SPEs) based on polymer matrices such as polyethylene oxide (PEO) and polyacrylonitrile and Li salts have higher flexibility and lower interface resistance and are more suitable for battery fabrication and application processes [18–21]. Unfortunately, their wide applications in solid-state LIBs are severely hindered by the low ion conductivity (10^{-7}–10^{-8}) at room temperature and poor mechanical and thermal stabilities [22–26].

A few strategies including constructing co-block [27,28] and cross-linking [29,30] polymers and adding plasticizers [31–33] are applied to tackle the problems of the SPEs, but there is a trade-off between the ion conductivity and the mechanical/thermal properties [24,30]. Another important route is to disperse ceramic nanoparticles including Al_2O_3 [34,35], SiO_2 [36], ZrO_2 [37] and TiO_2 [34,38] in the polymer matrices for preparing composite polymer electrolytes (CPEs), since this can improve both the ion conductivity and the mechanic/thermal properties [23]. Because of their large surface area and strong Lewis acid-base interaction with the electrolyte ion species, the inert ceramic nanoparticles can reduce the crystallization of the polymer matrices, facilitate the Li salt dissociation, and increase the ion conductivity [39].

* Corresponding author.
E-mail address: mcli@ncepu.edu.cn (M. Li).

https://doi.org/10.1016/j.ssi.2019.01.007
Received 8 October 2018; Received in revised form 14 December 2018; Accepted 4 January 2019

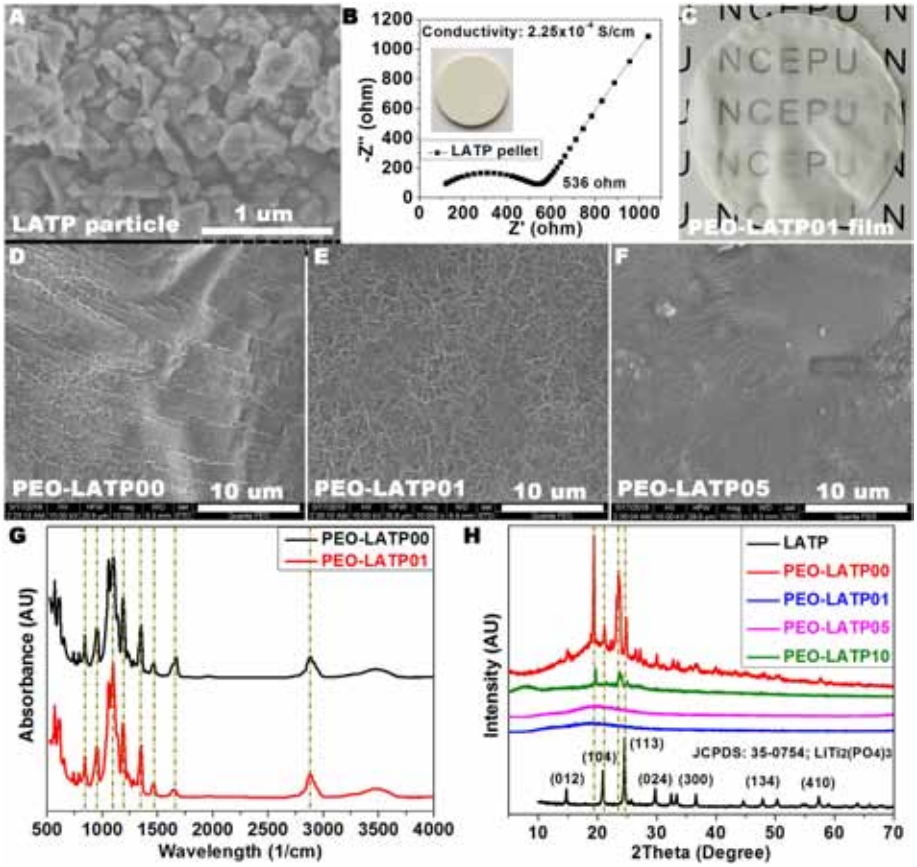

Fig. 1. (**A**) SEM image of the LATP nanoparticles, (**B**) EIS impedance of the LATP pellet, (**C**) optical photo of the PEO-LATP01 CPE film, surfacial SEM images of the (**D**) PEO-LATP00, (**E**) PEO-LATP01 and (**F**) PEO-LATP05 CPE films, and (**G**) FT-IR spectra and (**H**) XRD spectra of the PEO-LATP CPE films.

Finite element simulations also disclose the occurrence of ion conduction mostly at the ceramic-polymer interface [40–42]. Recently Li-containing ceramic electrolytes such as LLZO [43], LLTO [19], LAGP [14,21,44] and sulfides [45] were used as active fillers to furtherly enhance the ion conductivity based on the fast ion diffusion in the electrolyte particles and the suppression of polymer crystallization [46,47].

Herein, LATP electrolyte nanoparticle-filled CPE films with various LATP contents were developed. The ion conductivity, electrochemical window, mechanical and thermal properties, interfacial stability against Li dendrites, and the electrochemical properties of the CPE-based all-solid-state cells are studied in detail. It was shown that the Li ion conduction, mechanical and thermal stabilities, and the resistance against Li dendrites can be greatly improved by the addition of the active LATP nanoparticles into the PEO-LiTFSI membrane, and this also increased the specific capacity, capacity retention and rate capability of the all-solid-state cells.

2. Experimental

2.1. Chemicals and materials

Li_2CO_3, Al_2O_3, TiO_2 and $(NH_4)_2H(PO_4)_3$ with 99% purity were purchased from Alfa Aesar. PEO with molecular weight of 600,000 was obtained from Aldrich. Lithium bis(trifluoromethane) sulfonamide (LiTFSI) with 99% purity, *N*-methylpyrrolidone, anhydrous acetonitrile were purchased from Aladdin.

2.2. Preparation of LATP nanoparticles and PEO-LATP composite electrolytes

To synthesize $Li_{1.4}Al_{0.4}Ti_{1.6}(PO_4)_3$, a stoichiometric mixture of Li_2CO_3, Al_2O_3, TiO_2 and $(NH_4)_2H(PO_4)_3$ was firstly ball-milled at 400–600 rpm for 2 h in ethanol, and then heated in a alumina crucible at 80 °C for 3 h, 450 °C for 2 h and 900 °C for 4 h with a heating rate of 2 °C/min. The sintered samples were ball-milled in ethanol at 400–600 rpm/min for 4 h and dried at 60 °C for 12 h for LATP nanoparticles.

To prepare CPE films, PEO, LATP and LiTFSI powders with the EO/Li ratio of 16 and LATP content of 1–10 wt% were stirred in acetonitrile at 40 °C for 12 h. After that the mixture solutions were dropped in Teflon plates, and then dried in vacuum oven at 30 °C for 12 h and 50 °C for 12 h. The composite films with 0, 1, 5 and 10 wt% LATP were denoted as PEO-LATP00, PEO-LATP01, PEO-LATP05 and PEO-LATP10, respectively.

2.3. Characterization and measurements

The crystal structures of the LATP particles and CPE films were examined by a Bruker D8 Focus X-ray diffraction (XRD) analyzer (Cu K_α radiation, $\lambda = 0.154$ nm) at 10 °/min. The morphologies were taken by a FEI Quanta 200F scanning electron microscope (SEM). The FT-IR spectra were taken in a Frontier analyzer in a wavelength range of 500–4000 cm^{-1}. The thermal stability of the electrolyte films was measured by D840TA Q500 thermo-gravimetric analyzer (TGA) under Ar flow with a heating rate of 10 °C/min.

Stainless steel (SS)/CPE/Li, Li/CPE/Li and $LiFePO_4$/CPE/Li cells were assembled in a glove box under Ar protection. The $LiFePO_4$ cathodes were prepared by coating a slurry of $LiFePO_4$, carbon black

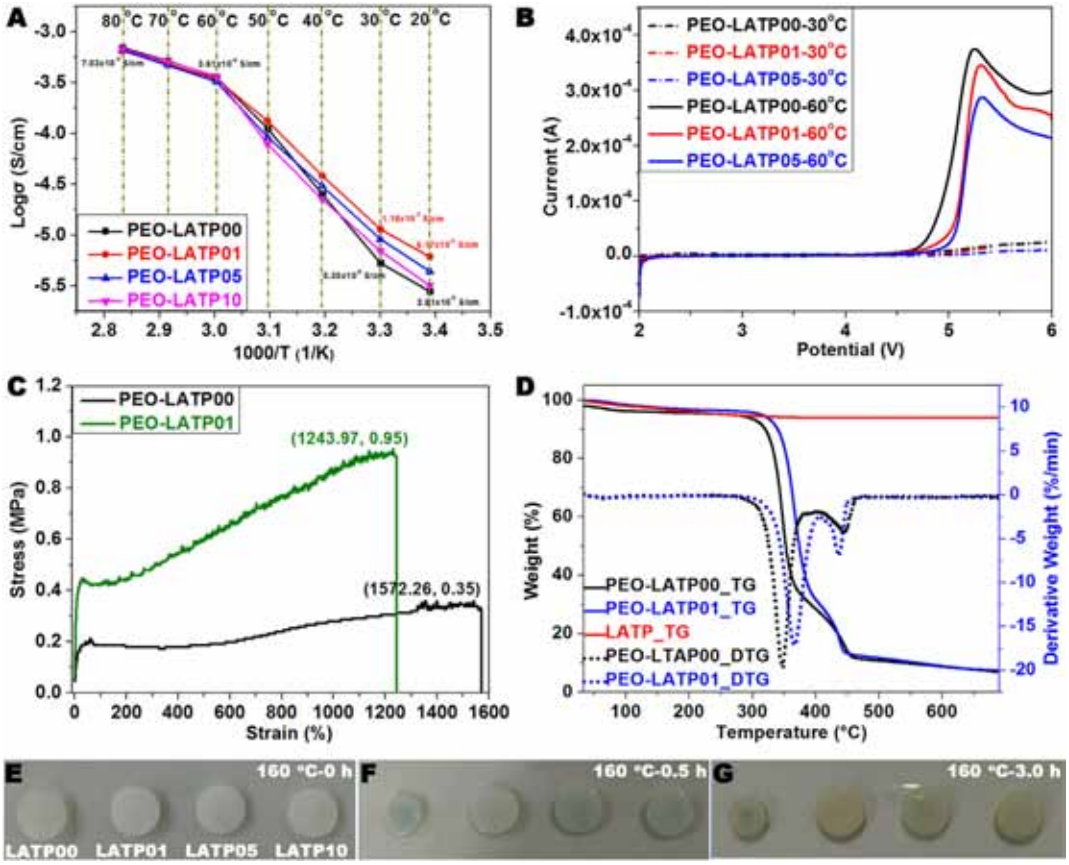

Fig. 2. (A) Ion conductivity at various temperatures, (B) linear sweep voltammetry profiles, (C) stress-strain curves, (D) TGA curves, and optical photos at 160 °C for (E) 0, (F) 0.5 and (G) 3.0 h in an oven of the PEO-LATP CPE films.

(CB) and PVDF at a weight ratio of 8:1:1 onto Al foils with ~2 mg/cm^2 mass loading. The electrochemical impedance spectroscopy (EIS) was measured at 20–80 °C using a Zahner Zennium electrochemical workstation in a frequency range of 10^6–10^{-2} Hz. The ion conductivity (σ) of the electrolyte films was calculated from the equation: $\sigma = L/SR$, where L, S and R represented the thickness, surface area and resistance of the electrolyte films, respectively. Cyclic voltammetry (CV) and linear sweep voltammetry (LSV) tests were performed on a CHI660E electrochemical workstation. Galvanostatic charge-discharge measurements were conducted in a Land LANHE CT2001A multichannel battery tester within 2.5–3.8 V (vs. Li/Li$^+$) under various temperatures and C rates (1 C = 150 mAh/g).

3. Results and discussion

3.1. Crystal structure and morphology

The ball-milled LATP particles had an average size of ~140 nm by counting the particle size in the SEM image (Fig. 1A). The LATP pellet showed a total resistance of 536 Ω, which corresponded to a high ion conductivity of 2.25 × 10^{-4} S/cm at 25 °C (Fig. 1B). The small size and high ion conductivity of the LATP particles were expected to effectively improve the properties of the CPE films. The CPE films with ≤10 wt% LATP were semi-transparent and flexible (Fig. 1C). A lot of wrinkles formed on the CPE films, and the LATP nanoparticles agglomerated when increasing the LATP content to 5 wt% (Fig. 1D–F). The aggregation of the LATP nanoparticles may affect the crystallization of PEO and the ion conductivity of the CPE films.

The FT-IR absorbance spectra of the electrolyte films were shown in Fig. 1G. The typical absorbance peaks at 2876 and 1095 cm^{-1} were assigned to the vibrations of C—H and C—O bonds of PEO. Compared the spectra of LATP-free film with the LATP-filled film, there were no obvious shifts and shape changes, indicating that the LATP nanoparticles were not forming complexes but mechanically dispersing in the PEO matrix. The LATP nanoparticles exhibited typical X-ray diffraction peaks same to $LiTi_2(PO_4)_3$ crystal (JCPDS card ID: 35–0754, Fig. 1H). A group of strong peaks at around 19.5 and 23.6° were obviously visible, suggesting the high crystallinity degree of the PEO matrix in the LATP-free film. These typical peaks disappeared in the PEO-LATP01 and PEO-LATP05 films, indicating the low PEO crystallinity in the films. However, the peaks at 19.5 and 23.6° (ascribed to PEO) and at 21.1 and 24.5° (may ascribed to (104) and (113) lattice planes of LATP) appeared again in the PEO-LATP10 film, which should be attributed to the much aggregation of the LATP nanoparticles and the resulted high PEO crystallinity.

3.2. Electrical, electrochemical, mechanical and thermal stabilities

The PEO-LATP01 CPE film showed much higher ion conductivities of 6.17 × 10^{-6} and 1.15 × 10^{-5} S/cm at 20 and 30 °C than the LATP-free film (2.81 × 10^{-6} and 5.35 × 10^{-6} S/cm, Fig. 2A), respectively, because of the high ion conductivity of LATP (Fig. 1B) and the inhibition of PEO crystallization by the LATP nanofillers (Fig. 1H). However, the CPE films with higher LATP contents had lower ion conductivities at room temperatures, which was ascribed to the much more agglomeration of the LATP nanoparticles and the increase of the PEO crystallinity (Fig. 1F and H). When the temperature increased to 60 and 80 °C, the ion conductivities of all the CPE films increased to around 3.61 × 10^{-4} and 7.03 × 10^{-4} S/cm, respectively, due to the transition from crystallization to amorphous state of the PEO matrices at ~60 °C [48].

The LATP-free film was electrochemically oxidized at around 5.0 V (vs. Li/Li$^+$) at 30 °C, but its electrochemical window decreased to

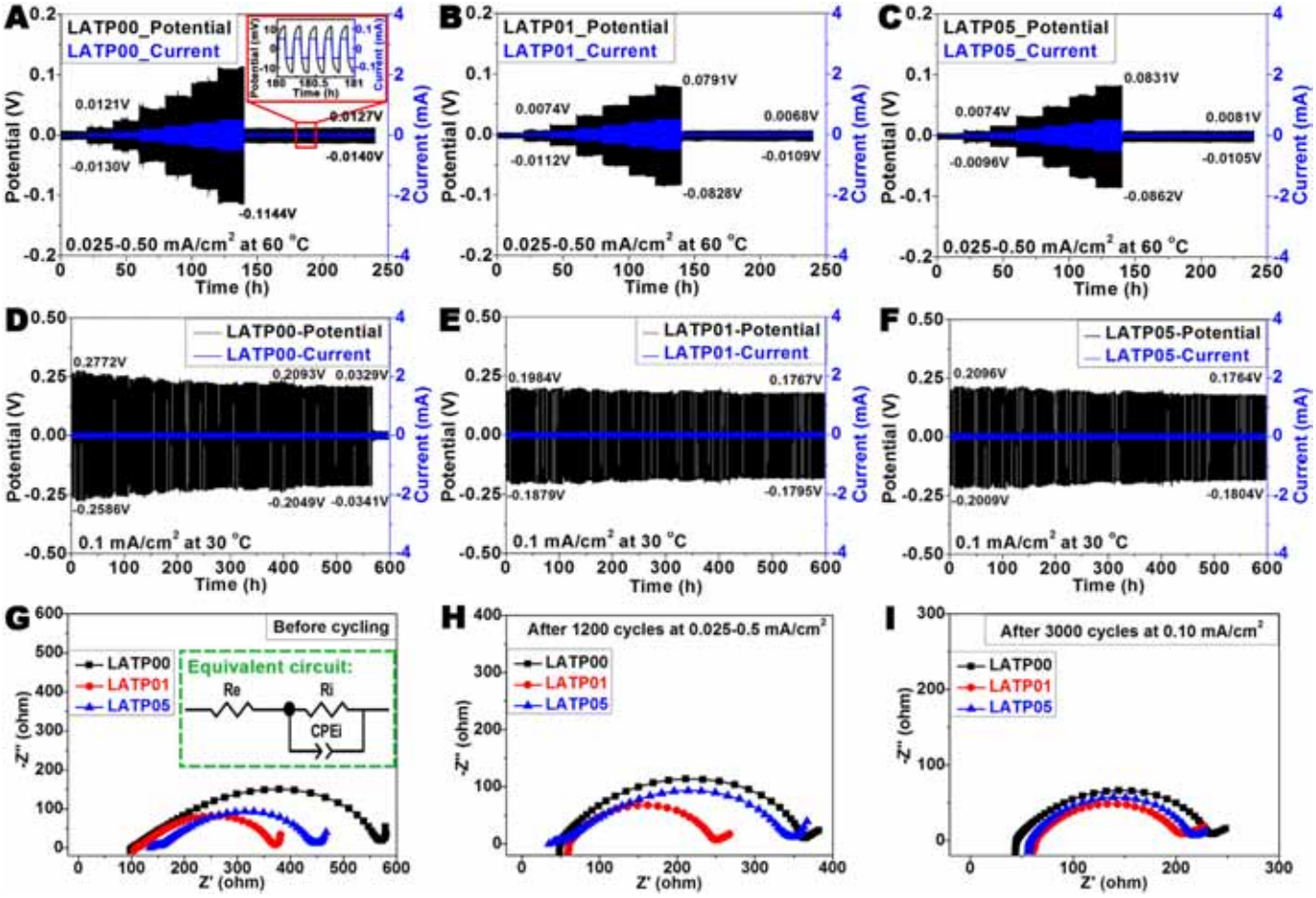

Fig. 3. Galvanostatic cycling curves of the (A) PEO-LATP00, (B) PEO-LATP01 and (C) PEO-LATP05 film-based Li/CPE/Li cells under various current densities of 0.025–0.50 mA/cm^2 for 240 h at 60 °C. Galvanostatic cycling curves of the (D) PEO-LATP00, (E) PEO-LATP01 and (F) PEO-LATP05 film-based Li/CPE/Li cells under various current densities of 0.10 mA/cm^2 for 600 h at 30 °C. EIS spectra at 50 °C of the Li/CPE/Li cells (G) before galvanostatic cycling and after (H) 1200 cycles at 0.025–0.50 mA/cm^2 and (I) 3000 cycles at 0.10 mA/cm^2.

around 4.5 V at 60 °C (Fig. 2B). However, when increasing the LATP content to 5 wt%, the electrochemical window increased to around 4.8 V, because of the wide electrochemical window of LATP [1]. The CPE film with 1 wt% LATP also exhibited higher ultimate tensile stress of 0.95 MPa and lower tensile strain of 1244% than the PEO-LiTFSI film (0.35 MPa and 1572%, Fig. 2C), indicating the better mechanical stability of the LATP-filled CPE films. Moreover, because of the incorporation of high-thermostability LATP fillers (with only obvious weight decrease of 4.0% before 200 °C due to water evaporation) into the polymer electrolyte, the PEO-LATP01 film had a higher decomposition temperature of 365.4 °C than the PEO-LITFSI film (347.2 °C, Fig. 2D), suggesting the higher thermal stability of the LATP-filled CPE films. The superior thermal stability of the LATP-filled films was furtherly proven by observing the shape and size changes of the films at 160 °C in air. The LATP-free sample began to melt after 0.5–3.0 h storage, but the LATP-filled films still kept the original shape and size (Fig. 2E–G).

3.3. Interfacial resistance against Li

The mechanical stability of the electrolyte films against Li dendrites was investigated using symmetric Li/CPE/Li cells. During the periodic charge-discharge processes, Li ions were plating/stripping the Li metal electrodes. When tested at 60 °C, the LATP-free cell showed an initial potential of 0.0121 V at 0.05 mA/cm^2, and the potential increased to 0.1135 V at 0.50 mA/cm^2 (Fig. 3A). After the current density returned to 0.05 mA/cm^2, the potential almost kept the same value (0.0127 V) even after 240 h. In comparison, the PEO-LATP01 and PEO-LATP05 film-based cells exhibited lower potentials than the LATP-free cell, suggesting that the lower interfacial resistances between the LATP-filled CPE films and Li metals (Fig. 3B–C). The PEO-LATP01 film-based cells also had the lowest potential among the samples.

When tested at a lower temperature of 30 °C, the LATP-free cells showed a higher potential of 0.2772 V at 0.10 mA/cm^2, and then the potential suddenly decreased to 0.0329 V after 567 h (Fig. 3D), implying the penetration of the electrolyte film by Li dendrites and short circuit of the cell [49,50]. However, no sudden potential drop was observed in the LATP-based cells even after 600 h (Fig. 3E–F), indicating that the LATP nanofillers may reinforce the PEO matrices and make them mechanically stronger. The potentials also slowly reduced from ~0.20 V to 0.18 V, due to the improved interface contact between the CPE films and Li metal electrodes during the repeated Li deposition process [51]. Besides, the LATP-based cells showed lower potential values than the LATP-free cells, furtherly proving the lower resistances of the LATP-filled CPE films.

EIS spectra were also used to investigate the impedance change of the Li/CPE/Li cells during the Li plating/stripping processes (Fig. 3G–I). An equivalent circuit model was utilized to fit the impedance plots. The semicircles at high and low frequencies were attributed to the ohmic resistance from the electrolytes (R_e) and the interfacial resistance between the electrolyte films and lithium metals (R_i), respectively [51,52]. The PEO-LATP01 film-based cell displayed lower total resistances of 252 and 208 Ω than the PEO-LATP00 and PEO-LATP05 film-based cells after 1200 cycles at 0.025–0.50 mA/cm^2 (373 and

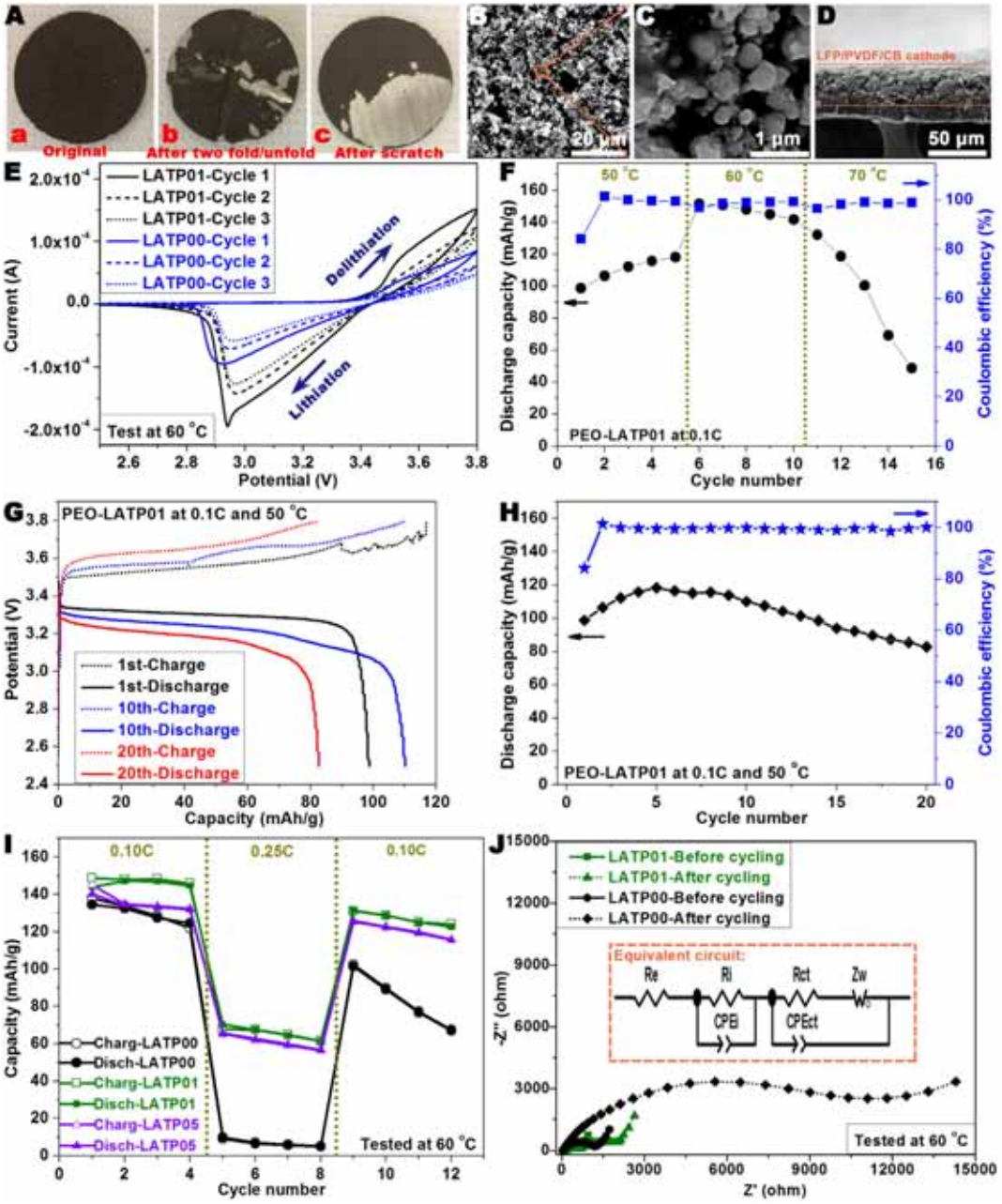

Fig. 4. (A) Optical images (a) before and after (b) two fold/unfold and (c) one scratch processes, and (B–C) surface and (D) cross-section SEM images of the $LiFePO_4$-PVDF-CB/Al electrode. (E) Cyclic voltammograms of the $LiFePO_4$/CPE/Li cells under 0.1 mV/s at 60 °C, and (F) cycling performance of the PEO-LATP01 film-based cells at 0.1 C under various operation temperatures. (G) Charge-discharge profiles and (H) cycling performance of the PEO-LATP01 film-based cells at 0.1 C and 50 °C. (I) Rate performance and (J) impedance curves of the $LiFePO_4$/CPE/Li cells at 60 °C.

286 Ω) and 3000 cycles at 0.10 mA/cm^2 (240 and 220 Ω), respectively. These findings about the Li plating/stripping showed that the 1 wt% LATP nano-filling can effectively reduce the interface resistance between the electrolyte film and Li metal electrodes and mechanically stabilize the PEO matrices, which were consistent with the impedance, mechanical tensile and thermal stability measurements (Fig. 2). Moreover, the 1% and 5% LATP-based cells showed decreasing R_i values from 270 and 315 Ω to 144 and 162 Ω after 3000 cycles at 0.10 mA/cm^2, respectively, because of the improved interface between the electrolyte films and Li metal electrodes, which furtherly explained the decrease in voltage (Fig. 3E–F) [50,51].

3.4. Cycling performance of the all-solid-state cells

The electrolyte films were also assembled in $LiFePO_4$/CPE/Li-structured coin cells for investigating their electrochemical properties. Olivine-structured $LiFePO_4$ cathode materials were usually used in all-solid-state batteries due to its relatively high thermal stability compared to the layered cathode materials. The dry slurries of $LiFePO_4$-PVDF-CB can be easily removed from the Al current collectors after the fold/unfold or scratch processes (Fig. 4A), which should originate from the low adhesive capability of the PVDF binder and the resulting loose construction in the electrodes and poor bonding strength between the electrode films and the Al foils (Fig. 4B–D). The cyclic voltammetry measurements showed that the oxidation and reduction peaks related to the delithiation/lithiation of $LiFePO_4$ appeared at around 3.6 and 3.0 V,

respectively, and the higher peak currents of the LATP-based cells suggested that the more rapid electrochemical reactions occurred in the Li-ion cells (Fig. 4E).

The $LiFePO_4$/CPE/Li cells were then electrochemically cycled at 0.10 C under various temperatures to disclose the effect of the operation temperature on the cycling performance (Fig. 4F). When increasing the temperature from 50 to 60 °C, the discharge capacity of the PEO-LATP01 film-based cells increased to 151.6 mAh/g, which was 89.2% of the theoretic capacity of $LiFePO_4$. However, the discharge capacity decreased to 132.1 mAh/g at 70 °C, and the capacity dropped much quickly during the continued cycling process. Such phenomenon also happened in other reports [28,53,54], which should be attributed to the low ionic conductivity and poor adhesive capability (Fig. 4A–B) of the PVDF binder, and the resulted high resistances of the cathode and the cathode/electrolyte interface [14]. The optimization of the cathode composition and constructure (e.g., flexible PEO with higher ionic conductivity and adhesive capability as binder, and use of high-strength carbon nano-additives to increase the mechanical strength) would be beneficial to improve the high-temperature cycling stability by decreasing the resistance and increasing the mechanical stability of the cathodes [14,28].

When the $LiFePO_4$/CPE/Li cells were cycled at 0.10 C under a lower temperature of 50 °C (Fig. 4G–H), two potential plateaus appeared at around 3.6 and 3.2 V (Fig. 4G), corresponded to the delithiation/lithiation processes of $LiFePO_4$. There was also a polarization during the continued charge-discharge processes, owing to the decomposition of $LiFePO_4$ at the high temperature and the charge transport kinetic limitations at the electrode-electrolyte interface [55]. Moreover, the PEO-LATP01 film-based cells exhibited initial reversible capacity of 98.7 mAh/g and Coulombic efficiency of 84.2% (Fig. 4H). The capacity and Coulombic efficiency increased to 118.3 mAh/g and 99.5% after the first five cycles, respectively, because of the penetration of the CPE into the cathode and the activation of $LiFePO_4$. The cells also maintained high capacity of 82.7 mAh/g and capacity retention of 84% after 20 cycles.

The rate performance of the $LiFePO_4$/CPE/Li cells was also evaluated at 60 °C (Fig. 4I). When increasing the charge-discharge rate from 0.10 C to 0.25 C, the capacity of the PEO-LATP01 film-based cells decreased from around 147 to 70 mAh/g. After the rate returned to 0.10 C, the capacity increased to 132 mAh/g with a capacity retention of 90% relative to the initial cycling at 0.1 C. The PEO-LATP05 film-based cells exhibited relatively low capacities of 140.2 and 65.3 mAh/g at 0.10 C and 0.25 C, respectively, owing to the relatively low ion conductivity of the PEO-LATP05 CPE. In sharp contrast, the LATP-free cells showed much lower capacities and capacity retentions at 0.10–0.25 C, because the LATP-free electrolyte film had lower ion conductivity (Fig. 2A) and higher interfacial resistance with the electrodes (Fig. 3).

EIS technology was then applied to study the impedance change during the charge-discharge process (Fig. 4J). An equivalent circuit model was used to fit the impedance plots. R_e, R_i and R_{ct} represent the bulk resistance of the electrolyte, the interfacial resistance, and the charge transfer resistance, respectively [56]. The LATP-based cells showed lower total resistances of 648 and 2050 Ω than the LATP-free cells (1200 and 11,100 Ω) before and after the electrochemical cycling at the various C rates, respectively, furtherly indicating the much rapid charge transfer inside the LATP-based cells [57–60], which was consistent with the cyclic voltammetry test (Fig. 4E).

4. Conclusions

LATP electrolyte nanoparticles were used to prepare PEO-LATP CPE films by solution casting. Because of the effective inhibition of the PEO crystallization, the CPE film with 1 wt% LATP showed the highest ion conductivity of 1.2×10^{-5} S/cm at room temperature. The electrochemical, mechanical and thermal stabilities were also enhanced by the active LATP nanofillers. The LATP-filled CPEs also exhibited superior interfacial stability against Li dendrites during the periodic Li plating/stripping (600 h at 0.10 mA/cm^2 and 30 °C), due to the improved conductivity and mechanical robustness. High capacity of 118.3 mAh/g and capacity retention of 84% were achieved in the LATP-based $LiFePO_4$/Li cells after 20 cycles at 50 °C.

Declarations of interest

None.

Acknowledgments

This work is supported partially by Beijing Natural Science Foundation (L172036), Joint Funds of the Equipment Pre-Research and Ministry of Education (6141A020225), Par-Eu Scholars Program, Science and Technology Beijing 100 Leading Talent Training Project, Beijing Municipal Science and Technology Project (Z161100002616039), China Postdoctoral Science Foundation (2018M631419), the Fundamental Research Funds for the Central Universities (2016JQ01, 2017ZZD02) and the NCEPU “Double First-Class” Graduate Talent Cultivation Program.

References

[1] A. Manthiram, X. Yu, S. Wang, Lithium battery chemistries enabled by solid-state electrolytes, Nat. Rev. Mater. 2 (2017) 1–16, https://doi.org/10.1038/natrevmats.2016.103.
[2] Y. Zhang, J. Lai, Y. Gong, Y. Hu, J. Liu, C. Sun, Z.L. Wang, A safe high-performance all-solid-state lithium-vanadium battery with a freestanding V_2O_5 nanowire composite paper cathode, ACS Appl. Mater. Interfaces 8 (2016) 34309–34316, https://doi.org/10.1021/acsami.6b10358.
[3] C. Sun, J. Liu, Y. Gong, D.P. Wilkinson, J. Zhang, Recent advances in all-solid-state rechargeable lithium batteries, Nano Energy 33 (2017) 363–386, https://doi.org/10.1016/j.nanoen.2017.01.028.
[4] L. Liu, J. Lyu, T. Li, T. Zhao, Well-constructed silicon-based materials as high-performance lithium-ion battery anodes, Nanoscale 8 (2016) 701–722, https://doi.org/10.1039/C5NR06278K.
[5] L. Liu, F. Xie, J. Lyu, T. Zhao, T. Li, B.G. Choi, Tin-based anode materials with well-designed architectures for next-generation lithium-ion batteries, J. Power Sources 321 (2016) 11–35, https://doi.org/10.1016/j.jpowsour.2016.04.105.
[6] L. Liu, J. Lyu, T. Zhao, T. Li, L. Liu, J. Lyu, T. Zhao, T. Li, Preparations and properties of porous copper materials for lithium-ion battery applications, Chem. Eng. Commun. 6445 (2016) 707–713, https://doi.org/10.1080/00986445.2015.1104504.
[7] L. Liu, B.G. Choi, S.O. Tung, T. Hu, Y. Liu, T. Li, T. Zhao, N.A. Kotov, Low-current field-assisted assembly of copper nanoparticles for current collectors, Faraday Discuss. 181 (2015) 383–401, https://doi.org/10.1039/C4FD00263F.
[8] C. Chen, Q. Li, Y. Li, Z. Cui, X. Guo, H. Li, Sustainable interfaces between Si anodes and garnet electrolytes for room-temperature solid-state batteries, ACS Appl. Mater. Interfaces 10 (2018) 2185–2190, https://doi.org/10.1021/acsami.7b16385.
[9] S.W. Song, K.C. Lee, H.Y. Park, High-performance flexible all-solid-state micro-batteries based on solid electrolyte of lithium boron oxynitride, J. Power Sources 328 (2016) 311–317, https://doi.org/10.1016/j.jpowsour.2016.07.114.
[10] A. Hammami, N. Raymond, M. Armand, Lithium-ion batteries: runaway risk of forming toxic compounds, Nature 424 (2003) 635–636, https://doi.org/10.1038/424635b.
[11] D. Wang, G. Zhong, Y. Li, Z. Gong, M.J. McDonald, J.-X. Mi, R. Fu, Z. Shi, Y. Yang, Enhanced ionic conductivity of $Li_{3.5}Si_{0.5}P_{0.5}O_4$ with addition of lithium borate, Solid State Ionics 283 (2015) 109–114, https://doi.org/10.1016/j.ssi.2015.10.009.
[12] X. Yao, B. Huang, J. Yin, G. Peng, Z. Huang, C. Gao, D. Liu, X. Xu, All-solid-state lithium batteries with inorganic solid electrolytes: review of fundamental science, Chinese Phys. B. 25 (2015) 1–14, https://doi.org/10.1088/1674-1056/25/1/018802.
[13] S. Wang, L. Ben, H. Li, L. Chen, Identifying Li^+ ion transport properties of aluminum doped lithium titanium phosphate solid electrolyte at wide temperature range, Solid State Ionics (2014), https://doi.org/10.1016/j.ssi.2014.10.004.
[14] Z. Zhang, Y. Zhao, S. Chen, D. Xie, X. Yao, P. Cui, X. Xu, An advanced construction strategy of all-solid-state lithium batteries with excellent interfacial compatibility and ultralong cycle life, J. Mater. Chem. A 5 (2017) 16984–16993, https://doi.org/10.1039/C7TA04320A.
[15] D.H. Kim, D.Y. Oh, K.H. Park, Y.E. Choi, Y.J. Nam, H.A. Lee, S.M. Lee, Y.S. Jung, Infiltration of solution-processable solid electrolytes into conventional Li-ion-battery electrodes for all-solid-state Li-ion batteries, Nano Lett. 17 (2017) 3013–3020, https://doi.org/10.1021/acs.nanolett.7b00330.
[16] R. Koerver, I. Aygün, T. Leichtweiß, C. Dietrich, W. Zhang, J.O. Binder, P. Hartmann, W.G. Zeier, J. Janek, Capacity fade in solid-state batteries: interphase formation and chemomechanical processes in nickel-rich layered oxide cathodes

and lithium thiophosphate solid electrolytes, Chem. Mater. 29 (2017) 5574–5582, https://doi.org/10.1021/acs.chemmater.7b00931.
[17] B. Zhang, R. Tan, L. Yang, J. Zheng, K. Zhang, S. Mo, Z. Lin, F. Pan, Mechanisms and properties of ion-transport in inorganic solid electrolytes, Energy Storage Mater. 10 (2018) 139–159, https://doi.org/10.1016/j.ensm.2017.08.015.
[18] Y. Tong, Y. Xu, D. Chen, Y. Xie, L. Chen, M. Que, Y. Hou, Deformable and flexible electrospun nanofiber-supported cross-linked gel polymer electrolyte membranes for high safety lithium-ion batteries, RSC Adv. 7 (2017) 22728–22734, https://doi.org/10.1039/C7RA00112F.
[19] J. Zhang, N. Zhao, M. Zhang, Y. Li, P.K. Chu, X. Guo, Z. Di, X. Wang, H. Li, Flexible and ion-conducting membrane electrolytes for solid-state lithium batteries: dispersion of garnet nanoparticles in insulating polyethylene oxide, Nano Energy 28 (2016) 447–454, https://doi.org/10.1016/j.nanoen.2016.09.002.
[20] W. Zhou, S. Wang, Y. Li, S. Xin, A. Manthiram, J.B. Goodenough, Plating a dendrite-free lithium anode with a polymer/ceramic/polymer sandwich electrolyte, J. Am. Chem. Soc. 138 (2016) 9385–9388, https://doi.org/10.1021/jacs.6b05341.
[21] C. Wang, Y. Yang, X. Liu, H. Zhong, H. Xu, Z. Xu, H. Shao, F. Ding, Suppression of lithium dendrite formation by using LAGP-PEO (LiTFSI) composite solid electrolyte and lithium metal anode modified by PEO (LiTFSI) in all-solid-state lithium batteries, ACS Appl. Mater. Interfaces 9 (2017) 13694–13702, https://doi.org/10.1021/acsami.7b00336.
[22] J. Zheng, M. Tang, Y.-Y. Hu, Lithium ion pathway within $Li_7La_3Zr_2O_{12}$-polyethylene oxide composite electrolytes, Angew. Chem. Int. Ed. 55 (2016) 12538–12542, https://doi.org/10.1002/anie.201607539.
[23] X. Zhang, T. Liu, S. Zhang, X. Huang, B. Xu, Y. Lin, B. Xu, L. Li, C.W. Nan, Y. Shen, Synergistic coupling between $Li_{6.75}La_3Zr_{1.75}Ta_{0.25}O_{12}$ and poly(vinylidene fluoride) induces high ionic conductivity, mechanical strength, and thermal stability of solid composite electrolytes, J. Am. Chem. Soc. 139 (2017) 13779–13785, https://doi.org/10.1021/jacs.7b06364.
[24] R. Bouchet, S. Maria, R. Meziane, A. Aboulaich, L. Lienafa, J.P. Bonnet, T.N.T. Phan, D. Bertin, D. Gigmes, D. Devaux, R. Denoyel, M. Armand, Single-ion BAB triblock copolymers as highly efficient electrolytes for lithium-metal batteries, Nat. Mater. 12 (2013) 452–457, https://doi.org/10.1038/nmat3602.
[25] Y. Tong, L. Chen, Y. Chen, X. He, Enhanced conductivity of novel star branched liquid crystalline copolymer based on poly(ethylene oxide) for solid polymer electrolytes, Appl. Surf. Sci. 258 (2012) 10095–10103, https://doi.org/10.1016/j.apsusc.2012.06.082.
[26] J. Bao, X. Qu, G. Qi, Q. Huang, S. Wu, C. Tao, M. Gao, C. Chen, Solid electrolyte based on waterborne polyurethane and poly(ethylene oxide) blend polymer for all-solid-state lithium ion batteries, Solid State Ionics 320 (2018) 55–63, https://doi.org/10.1016/j.ssi.2018.02.030.
[27] Q. Wang, W.L. Song, L.Z. Fan, Y. Song, Flexible, high-voltage and free-standing composite polymer electrolyte membrane based on triethylene glycol diacetate-2-propenoic acid butyl ester copolymer for lithium-ion batteries, J. Membr. Sci. 492 (2015) 490–496, https://doi.org/10.1016/j.memsci.2015.06.041.
[28] L. Porcarelli, A.S. Shaplov, M. Salsamendi, J.R. Nair, Y.S. Vygodskii, D. Mecerreyes, C. Gerbaldi, Single-ion block copoly(ionic liquid)s as electrolytes for all-solid state lithium batteries, ACS Appl. Mater. Interfaces 8 (2016) 10350–10359, https://doi.org/10.1021/acsami.6b01973.
[29] R. Khurana, J.L. Schaefer, L.A. Archer, G.W. Coates, Suppression of lithium dendrite growth using cross-linked polyethylene/poly(ethylene oxide) electrolytes: a new approach for practical lithium-metal polymer batteries, J. Am. Chem. Soc. 136 (2014) 7395–7402, https://doi.org/10.1021/ja502133j.
[30] Q. Lu, Y.B. He, Q. Yu, B. Li, Y.V. Kaneti, Y. Yao, F. Kang, Q.H. Yang, Dendrite-free, high-rate, long-life lithium metal batteries with a 3D cross-linked network polymer electrolyte, Adv. Mater. 29 (2017), https://doi.org/10.1002/adma.201604460.
[31] C.-W. Nan, L. Fan, Y. Lin, Q. Cai, Enhanced ionic conductivity of polymer electrolytes containing nanocomposite SiO_2 particles, Phys. Rev. Lett. 91 (2003) 266104, , https://doi.org/10.1103/PhysRevLett.91.266104.
[32] R. He, T. Kyu, Effect of plasticization on ionic conductivity enhancement in relation to glass transition temperature of crosslinked polymer electrolyte membranes, Macromolecules 49 (2016) 5637–5648, https://doi.org/10.1021/acs.macromol.6b00918.
[33] B. Chen, Z. Huang, X. Chen, Y. Zhao, Q. Xu, P. Long, S. Chen, X. Xu, A new composite solid electrolyte PEO/$Li_{10}GeP_2S_{12}$/SN for all-solid-state lithium battery, Electrochim. Acta 210 (2016) 905–914, https://doi.org/10.1016/j.electacta.2016.06.025.
[34] F. Croce, G.B. Appetecchi, L. Persi, B. Scrosati, Nanocomposite polymer electrolytes for lithium batteries, Nature 394 (1998) 456–458, https://doi.org/10.1038/28818.
[35] E.M. Masoud, A.A. El-Bellihi, W.A. Bayoumy, M.A. Mousa, Organic–inorganic composite polymer electrolyte based on PEO–$LiClO_4$ and nano-Al_2O_3 filler for lithium polymer batteries: dielectric and transport properties, J. Alloy. Compd. 575 (2013) 223–228, https://doi.org/10.1016/j.jallcom.2013.04.054.
[36] S. Liu, H. Wang, N. Imanishi, T. Zhang, A. Hirano, Y. Takeda, O. Yamamoto, J. Yang, Effect of co-doping nano-silica filler and *N*-methyl-*N*-propylpiperidinium bis(trifluoromethanesulfonyl)imide into polymer electrolyte on Li dendrite formation in Li/poly(ethylene oxide)-Li$(CF_3SO_2)_2$N/Li, J. Power Sources 196 (2011) 7681–7686, https://doi.org/10.1016/j.jpowsour.2011.04.001.
[37] W. Liu, D. Lin, J. Sun, G. Zhou, Y. Cui, Improved lithium ionic conductivity in composite polymer electrolytes with oxide-ion conducting nanowires, ACS Nano 10 (2016) 11407–11413, https://doi.org/10.1021/acsnano.6b06797.
[38] A.R. Polu, H.-W. Rhee, Effect of TiO_2 nanoparticles on structural, thermal, mechanical and ionic conductivity studies of PEO_{12}-LiTDI solid polymer electrolyte, J. Ind. Eng. Chem. 37 (2016) 347–353, https://doi.org/10.1016/j.jiec.2016.03.042.
[39] J. Cao, L. Wang, X. He, M. Fang, J. Gao, J. Li, L. Deng, H. Chen, G. Tian, J. Wang, S. Fan, In situ prepared nano-crystalline TiO_2-poly(methyl methacrylate) hybrid enhanced composite polymer electrolyte for Li-ion batteries, J. Mater. Chem. A 1 (2013) 5955, https://doi.org/10.1039/c3ta00086a.
[40] W.E. Tenhaeff, X. Yu, K. Hong, K.A. Perry, N.J. Dudney, Ionic transport across interfaces of solid glass and polymer electrolytes for lithium ion batteries, J. Electrochem. Soc. 158 (2011) A1143–A1149, https://doi.org/10.1149/1.3625281.
[41] S. Kalnaus, A.S. Sabau, W.E. Tenhaeff, N.J. Dudney, C. Daniel, Design of composite polymer electrolytes for Li ion batteries based on mechanical stability criteria, J. Power Sources 201 (2012) 280–287, https://doi.org/10.1016/j.jpowsour.2011.11.020.
[42] S. Kalnaus, W.E. Tenhaeff, J. Sakamoto, A.S. Sabau, C. Daniel, N.J. Dudney, Analysis of composite electrolytes with sintered reinforcement structure for energy storage applications, J. Power Sources 241 (2013) 178–185, https://doi.org/10.1016/j.jpowsour.2013.04.096.
[43] J.H. Choi, C.H. Lee, J.H. Yu, C.H. Doh, S.M. Lee, Enhancement of ionic conductivity of composite membranes for all-solid-state lithium rechargeable batteries incorporating tetragonal $Li_7La_3Zr_2O_{12}$ into a polyethylene oxide matrix, J. Power Sources 274 (2015) 458–463, https://doi.org/10.1016/j.jpowsour.2014.10.078.
[44] Y.-C. Jung, S.-M. Lee, J.-H. Choi, S.S. Jang, D.-W. Kim, All solid-state lithium batteries assembled with hybrid solid electrolytes, J. Electrochem. Soc. 162 (2015) A704–A710, https://doi.org/10.1149/2.0731504jes.
[45] Y. Zhao, C. Wu, G. Peng, X. Chen, X. Yao, Y. Bai, F. Wu, S. Chen, X. Xu, A new solid polymer electrolyte incorporating $Li_{10}GeP_2S_{12}$ into a polyethylene oxide matrix for all-solid-state lithium batteries, J. Power Sources 301 (2016) 47–53, https://doi.org/10.1016/j.jpowsour.2015.09.111.
[46] N.M. Asl, J. Keith, C. Lim, L. Zhu, Y. Kim, Inorganic solid/organic liquid hybrid electrolyte for use in Li-ion battery, Electrochim. Acta 79 (2012) 8–16, https://doi.org/10.1016/j.electacta.2012.06.038.
[47] S.S. Lee, Y.J. Lim, H.W. Kim, J.K. Kim, Y.G. Jung, Y. Kim, Electrochemical properties of a ceramic-polymer-composite-solid electrolyte for Li-ion batteries, Solid State Ionics 284 (2016) 20–24, https://doi.org/10.1016/j.ssi.2015.11.020.
[48] R.-J. Chen, Y.-B. Zhang, T. Liu, B.-Q. Xu, Y.-H. Lin, C.-W. Nan, Y. Shen, Addressing the interface issues in all-solid-state bulk-type lithium ion battery via an all-composite approach, ACS Appl. Mater. Interfaces 9 (2017) 9654–9661, https://doi.org/10.1021/acsami.6b16304.
[49] T. Yang, J. Zheng, Q. Cheng, Y.-Y. Hu, C.K. Chan, Composite polymer electrolytes with $Li_7La_3Zr_2O_{12}$ garnet-type nanowires as ceramic fillers: mechanism of conductivity enhancement and role of doping and morphology, ACS Appl. Mater. Interfaces 9 (2017) 21773–21780, https://doi.org/10.1021/acsami.7b03806.
[50] X. Ke, Y. Cheng, J. Liu, L. Liu, N. Wang, J. Liu, C. Zhi, Z. Shi, Z. Guo, Hierarchically bicontinuous porous copper as advanced 3D skeleton for stable lithium storage, ACS Appl. Mater. Interfaces 10 (2018) 13552–13561, https://doi.org/10.1021/acsami.8b01978.
[51] K. Fu, Y. Gong, J. Dai, A. Gong, X. Han, Y. Yao, C. Wang, Y. Wang, Y. Chen, C. Yan, Y. Li, E.D. Wachsman, L. Hu, Flexible, solid-state, ion-conducting membrane with 3D garnet nanofiber networks for lithium batteries, Proc. Natl. Acad. Sci. 113 (2016) 7094–7099, https://doi.org/10.1073/pnas.1600422113.
[52] J. Bae, Y. Li, F. Zhao, X. Zhou, Y. Ding, G. Yu, Designing 3D nanostructured garnet frameworks for enhancing ionic conductivity and flexibility in composite polymer electrolytes for lithium batteries, Energy Storage Mater. 15 (2018) 46–52, https://doi.org/10.1016/j.ensm.2018.03.016.
[53] B. Qin, Z. Liu, G. Ding, Y. Duan, C. Zhang, G. Cui, A single-ion gel polymer electrolyte system for improving cycle performance of $LiMn_2O_4$ battery at elevated temperatures, Electrochim. Acta 141 (2014) 167–172, https://doi.org/10.1016/j.electacta.2014.07.004.
[54] G.P. Pandey, S.A. Klankowski, T. Liu, J. Wu, J. Li, Toward highly stable solid-state unconventional thin-film battery-supercapacitor hybrid devices: interfacing vertical core-shell array electrodes with a gel polymer electrolyte, J. Power Sources 342 (2017) 1006–1016, https://doi.org/10.1016/j.jpowsour.2017.01.022.
[55] S. Wang, A. Wang, X. Liu, H. Xu, J. Chen, L. Zhang, Ordered mesogenic units-containing hyperbranched star liquid crystal all-solid-state polymer electrolyte for high-safety lithium-ion batteries, Electrochim. Acta 259 (2018) 213–224, https://doi.org/10.1016/j.electacta.2017.10.163.
[56] W. Zhang, J. Nie, F. Li, Z.L. Wang, C. Sun, A durable and safe solid-state lithium battery with a hybrid electrolyte membrane, Nano Energy 45 (2018) 413–419, https://doi.org/10.1016/j.nanoen.2018.01.028.
[57] L. Liu, B.G. Choi, S.O. Tung, J. Lyu, T. Li, T. Zhao, N.A. Kotov, Materials engineering of high-performance anodes as layered composites with self-assembled conductive networks, J. Phys. Chem. C 122 (2018) 14014–14028, https://doi.org/10.1021/acs.jpcc.8b01105.
[58] L. Liu, M. Li, J. Lyu, T. Zhao, T. Li, Facile and green preparation of three-dimensionally nanoporous copper films by low-current electrical field-induced assembly of copper nanoparticles for lithium-ion battery applications, J. Mater. Eng. Perform. 27 (2018) 4680–4692, https://doi.org/10.1007/s11665-018-3583-4.
[59] J. Liu, Y. Cheng, Q. Fan, L. Zhang, L. Liu, X. Ke, N. Wang, Z. Shi, Z. Guo, Trifunctional coating to enhance the capacity retention of $LiNi_{0.5}Mn_{1.5}O_4$ for high power lithium ion battery, Mater. Lett. 214 (2018) 68–71, https://doi.org/10.1016/j.matlet.2017.11.046.
[60] L. Liu, W. Xiao, J. Guo, Y. Cui, X. Ke, W. Cai, J. Liu, Y. Chen, Z. Shi, S. Chou, Nanocomposite $LiFePO_4$·$Li_3V_2(PO_4)_3$/C synthesized by freeze-drying assisted sol-gel method and its magnetic and electrochemical properties, Sci. China Mater. 61 (2018) 39–47, https://doi.org/10.1007/s40843-017-9114-0.